RESEARCH PAPERS

Acta Cryst. (1995). D**51**, 859–870

Laue Diffraction Studies of Human Rhinovirus 14 and Canine Parvovirus

BY ANDREA HADFIELD* AND JANOS HAJDU

Laboratory of Molecular Biophysics and Oxford Centre for Molecular Sciences, Rex Richards Building, South Parks Road, Oxford OX1 3QU, England

AND MICHAEL S. CHAPMAN† AND MICHAEL G. ROSSMANN

Department of Biological Sciences, Purdue University, West Lafayette, Indiana 47907, USA

(*Received* 3 *November* 1994; *accepted* 1 *March* 1995)

Abstract

Laue diffraction data have been collected from monoclinic crystals of canine parvovirus (CPV), and from cubic crystals of human rhinovirus 14 (HRV14) with and without bound antiviral compounds. In optimal conditions one or two images of HRV14 were sufficient to calculate interpretable electron-density maps of the virus complexes at 3.5 Å resolution. The crystals of CPV were of lower symmetry and were more easily damaged by radiation, making it difficult to accumulate a significant amount of useful data. Results on HRV14 are compared in studies on four antiviral compounds where data were collected using both monochromatic and Laue diffraction. Two Laue diffraction images of HRV14 with a point mutation were sufficient to determine the change from a leucine to a valine in VP2.

Introduction

Spherical virus particles often crystallize in high-symmetry space groups. With a cubic system it is theoretically possible to capture over 90% of the unique data set on a single polychromatic diffraction photograph (Clifton, Elder & Hajdu, 1991). In other space groups a relatively high proportion of the unique data set may still be recorded, although it could take a few images using different orientations of the crystal to collect a whole data set. High-symmetry space groups and the high non-crystallographic symmetry that is inherent in icosahedral virus crystals (Fig. 1) raise the possibility of obtaining high-quality electron-density maps from a single Laue diffraction image (Campbell *et al.*, 1990; Hajdu *et al.*, 1989). The Laue technique has previously been used to examine the effect of calcium binding to the plant virus tomato bushy stunt virus (TBSV) (Campbell *et al.*, 1990). A combination of Laue diffraction and difference methods could prove an efficient means of studying conformational changes associated with ligand binding (*e.g.* antiviral compounds), with pH or with mutations in the protein coat. Such studies are central to an understanding of virus cell attachment, penetration and uncoating.

The animal virus particles studied in this paper have a diameter of about 300 Å and thus form crystals with large unit cells, resulting in very densely populated diffraction patterns. Reflections which are overlapped need to be given special consideration since, in general, they will form a high proportion of the data set (Hadfield, 1992; Shrive, Clifton, Hajdu & Greenhough, 1990; Wakatsuki, 1993). Large unit-cell dimensions also lead to a proportional reduction in the intensity of each reflection

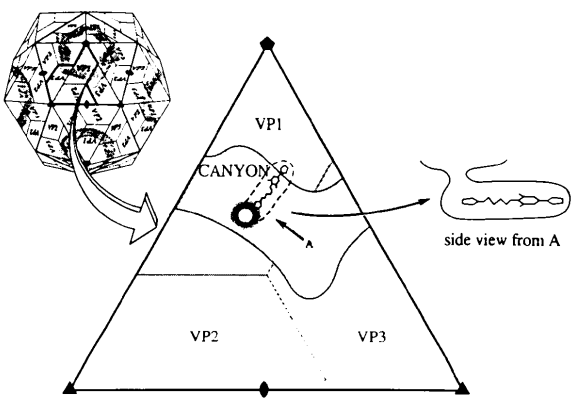

Fig. 1. A schematic diagram of an icosahedral virus capsid showing twofold, threefold and fivefold icosahedral symmetry axes. An enlargement of one icosahedral asymmetric unit of HRV14 shows the outline of the canyon and the entrance to the antiviral compound binding pocket. This corresponds to the orientation of the binding pocket in the following figures. The positions of viral proteins VP1, 2 and 3 are indicated. The 'canyon', a depression around the fivefold axis observed in HRV14 and other picornaviruses, is shaded in grey (Oliveira *et al.*, 1993).

* Present address: Department of Biological Sciences, Purdue University, West Lafayette, Indiana 47907, USA.

† Present address: Department of Chemistry and Institute of Molecular Biophysics, Florida State University, Tallahassee, Florida 32306, USA.

ISSN 0907-4449

Table 1. *Laue virus data collection*

Synchrotron (beamline)	Date	λ range (Å)	Exposure time (s)	Virus	No. of crystals exposed	Processable images	Resolution obtained (Å)	Mono. resolution (Å)	Comments
SRS (9.7)	Sept. 1988	0.25–2.1	10	HRV14+ compounds	9	1	4.0	2.8	Very weak, slightly streaked
SRS (9.7)	Sept. 1988	0.25–2.1	10	CPV native	5	0	—	3.0	Very poor
DESY (X31)	April 1990	0.65–1.7	4 × 10	HRV14+ compounds	6	0	—	2.8	Very poor. Crystals showed extensive damage
			20–120	CPV native	4	0	—	3.0	Very poor. Crystals showed extensive damage
CHESS (B2)	June 1990	0.7–1.4	3 + 4	HRV14 mutants	16	5	3.5	2.8	Some good diffraction. Quite weak, slight streaking
			3 + 4	CPV native	7	2	3.5	3.0	Quite weak, slightly streaked
SRS (9.7)	Aug. 1990	0.25–2.1	9	HRV14+ compounds	8	0	—	2.8	Very poor. Crystals showed damage
			5	CPV native	10	1	?	3.0	Good diffraction. Could not be indexed
SRS (9.7)	Sept. 1991	0.30–1.5	3 × 1–6 × 2	HRV14+ compounds	23	4	3.5	2.8	Weak, slightly streaked
SRS (9.5)	Sept. 1991	0.45–1.7	3 × 1.5	HRV14+ compounds	6	3	3.5	2.8	Quite weak, slightly streaked

for a given size of crystal. In addition, crystals of animal viruses tend to be more sensitive to radiation damage than those of plant or insect viruses. However, symmetry averaging can increase the signal-to-noise ratio in electron-density maps and reduce the amount of the complete data necessary to obtain an interpretable electron-density map. Two very different viruses, canine parvovirus (CPV; tetragonal crystals, 30-fold non-crystallographic symmetry) and human rhinovirus 14 (HRV14; cubic crystals, 20-fold non-crystallographic symmetry), were chosen to investigate the usefulness of Laue diffraction data collection in the study of icosahedral animal viruses. Details of some of the structural results are published elsewhere (reviewed in Chapman, Giranda & Rossmann, 1990).

Data collection

Data collection was performed at a number of different synchrotrons [Synchrotron Radiation Source (SRS), Daresbury; Cornell High Energy Synchrotron Source (CHESS), Ithaca; Deutsches Elektronen Synchrotron (DESY), Hamburg] using crystals grown at Purdue University (Table 1). The antiviral compounds, which were soaked into the crystals prior to exposure to X-rays (Smith *et al.*, 1986), were provided by the Sterling Winthrop Research Institute and also by the Janssen Research Foundation. Cooling was provided on the beamline at each synchrotron to keep the crystals near 277 K. Cooling reduces the rate of deterioration of the crystals in the X-ray beam and is used routinely for monochromatic data collection. During Laue data collection the crystals failed to show useful diffraction in the absence of cooling. All the diffraction images were collected on film (CEA Reflex 25, Kodak DEF 5) as this was the only medium available that allowed fine raster scanning (0.025 mm raster size). The films typically had about 200 000 diffraction spots in an area 11 × 11 cm. Small collimators (100–150 μm in diameter) were used to reduce overlap between reflections. A helium path between the sample and the backstop reduced absorption and background scatter.

The initial experiments were performed at the SRS on beamline 9.7, using small crystals which had been soaked with a variety of antiviral compounds. One of nine images a single exposure gave data which could be processed. This film pack (20*A* to *F*) was used to obtain maps for the antiviral compound WIN 54954 bound to HRV14. The resolution of the data was 4 Å, lower than that obtained by monochromatic oscillation photography, which was at least 2.8 Å. The following experiments, performed at DESY on beamline X31 in 1989, were non-productive because a weak beam necessitated long exposure times which led to excessive radiation damage. Data were collected next at CHESS from crystals of drug-resistant mutants of HRV14. Of the 16 Laue diffraction photographs taken five were judged worthy of indexing and integration, although they were weak and streaked to varying degrees. In contrast, nearly every photograph taken of these crystals with monochromatic radiation would have yielded useful diffraction data. There was a mirror in the beamline optics at CHESS which reduced the effective wavelength spread compared to that on beamlines 9.5 and 9.7 at the SRS. Each image was the result of several short exposures interspersed with cooling periods of a few seconds to reduce crystal overheating. In further experiments at the SRS the experimental procedure was changed in line with the observations made during the CHESS data-collection trip. The exposures were broken into small bursts with short spells of cooling in between and the wavelength range over which data were collected was reduced. A 0.1 mm thick aluminium filter was used to cut out much of the long wavelength radiation on station 9.7. Station 9.5 uses a focusing mirror which gives a relatively sharp cutoff below 0.45 Å and aluminium foil was inserted into the beam to diminish, but not completely block, radiation at the long end of the spectrum. The data

on good films now extended to 3.5 Å resolution and the number of processable films obtained was increased relative to previous data collections at the SRS (Fig. 2).

Data processing

The first stage in the data processing was carried out using software developed through the UK Collaborative Computational Project in Protein Crystallography (*CCP*4) by Pella Machin and co-workers (Helliwell *et al.*, 1989). The film was indexed using the programs *SPOTIN* and *ANALAUE* (Clifton *et al.*, 1991). After position and orientation refinement, reflections were predicted using the program *GENLAUE*. Diffraction spots stimulated by more than one wavelength in the same position on the film are multiplets. Spots with a centre-to-centre separation of less than the spot size (δ) were considered to be overlapped and were deconvoluted. Diffraction spots with a centre separation of less than $\varepsilon(\varepsilon < \delta)$, and those which were both multiplets and overlapped, were excluded. The diffraction spots were integrated using *INTLAUE* (Greenhough & Suddath, 1986; Shrive *et al.*, 1990). Where a whole film pack was used the films were scaled together using *AFSCALE*, which employed an empirically determined absorption curve for X-ray film (Clifton *et al.*, 1985). A high sigma cutoff [$I = 4$–$6(\sigma)I$] was used to select reflections for wavelength normalization. The intensities of the reflections were normalized by comparison of symmetry-related reflections recorded on the same film at different wavelengths (*LAUENORM*). Normalization of the reflections proved difficult, particularly for short wavelengths where intensities are weak (Fig. 3). The quality of the normalization results was measured as an R factor (R_L) representing the discrepancy between scaled individual intensities and their averaged values (Tables 2 and 3).

Table 2. *Data reduction for CPV films* 31 *and* 32

Process	Film 31	Film 32
Reflections predicted	58657	39006
Multiplets	4537	3211
Spatial overlaps ($\delta < 0.15$ mm)	43695	26755
Not deconvolutable ($\varepsilon < 0.09$ mm)	19058	9752
Both multiplet and overlapped	2986	1759
Integrable spots predicted	36354	26315
Integrated spots	33107	—
Unique reflections	8896	—
R_L*	0.211	—
% Complete unique data predicted	8	12
% Complete unique data extracted	3.2	0

* $R_L = [\sum_h \sum_i |(\langle I_h \rangle - sI_{hi})|]/(\sum_h \sum_i \langle I_h \rangle)$, where I_{hi} = polychromatic intensity at wavelength λ, I_h = normalized intensity, s = scale factor for I at wavelength λ.

Once the structure-factor amplitudes had been normalized with respect to wavelength, the rest of the data processing was performed using programs written at Purdue University. The data set was scaled to monochromatic native data in shells of intensity and resolution (*MGRSCALE*) (Rossmann, Leslie, Abdel-Meguid Tsukihara, 1979), which gave better results than the wavelength scaling (R_M in Table 3). The R_M values obtained were not substantially larger than R_{merge} values obtained from monochromatic oscillation photography (Arnold *et al.*, 1987). Since the resolution and wavelength are coupled in Laue data collection, scaling of Laue data to monochromatic data is roughly equivalent to finding a Laue normalization curve using an external standard. Further improvements might have been obtained by using the monochromatic data directly for obtaining a normalization curve.

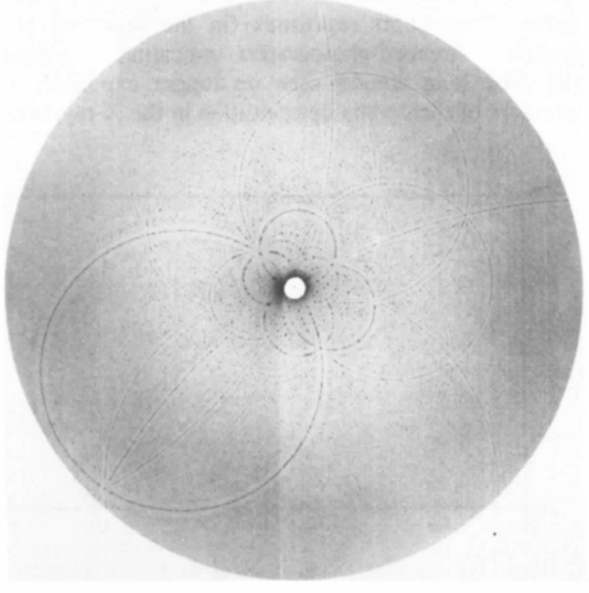

Fig. 2. Laue diffraction photograph of HRV14 incubated with R77975 taken at SRS, Daresbury, using a 100 µm collimator. The effective wavelength range was 0.45–1.7 Å. The crystal diffracted to around 3.5 Å resolution.

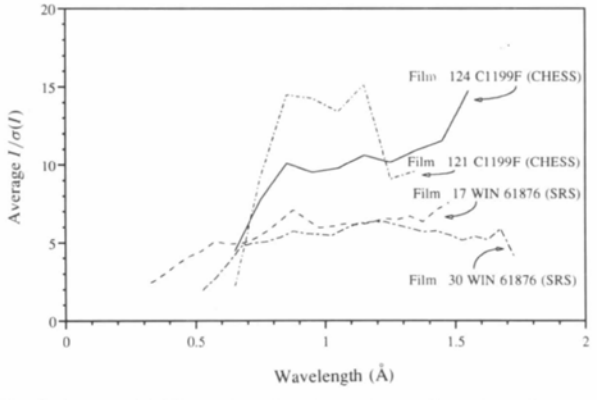

Fig. 3. Average $I/\sigma(I)$ as a function of wavelength for various data sets. The labels show the number of the film from which the data were extracted, and the sample from which the data were collected. The quality of the data at short wavelengths is consistently less. The quality of data is greatest when the data are collected using a truncated wavelength range.

Table 3. *Summary of HRV14 data processing*

	WIN 54954	R 61837	R 77975	WIN 61876			C1199→F		
Film No.*	20 (*A* to *F*)	52 (*A* to *F*)	34 (*A*)	30 (*A*)	17 (*A*)	Merged	124 (*A*)	121 (*A*)	Merged
Crystal-to-film distance (mm)	279	277.5	228.5	228.5	277.61	—	280	280	—
Spots predicted	214053	128842	215880	235390	224684	—	60451	63993	—
% Unique data predicted to 3.5 Å	58	61	54	54	57	—	31	32	—
Multiplets	—	22096	23895	27911	30254	—	11135	9818	—
Overlapped spots	118285	124618	195835	214998	201161	—	30609	48260	—
Both multiplet and overlapped	57318	15884	18467	22380	22545	—	5063	7457	—
Integrated spots (good spots)	148367	113214	192285	207784	196267	—	52537	55714	—
Unique reflections	17619	24447	45462	34677	46707	70609	29856	19235	45352
R_I (wavelength normalization) (%)†	26.7	20.3	15.5	15.5	17.8	16.9	15.7	13.4	—
% Unique data extracted to 3.5 Å	7.4	8.7	12.6	9.6	11.4	19.6	8.3	8	12.6
R_M (scaling to monochromatic data) (%)‡	15.6	12.9	11.3	—	—	10.8	11.8	—	9.6
Unique reflections accepted ($F > 4\sigma_F F$)	10512	15603	34015	—	—	50729	22842	—	36248

* (*A* to *F*) indicates that all films *A*, *B*, *C*, *D*, *E* and *F* within a film pack were used and merged. (*A*) indicates that only the top film of the film pack was used.

† $R_I = [\sum_h \sum_i |(\langle I_h \rangle - sI_{hi})|]/(\sum_h \sum_i \langle I_H \rangle)$ where I_h is the normalized intensity, I_{hi} is the intensity at wavelength λ and s is the scale factor for I_{hi} at wavelength λ.

‡ $R_M = [\sum_h \sum_i |(\langle I_{Mh} \rangle - sI_{hi})|]/(\sum_h \sum_i \langle I_{Mh} \rangle)$ where I_{Mh} is the monoclinic intensity, I_{hi} is the normalized Laue intensity and s is the scale factor for I_{hi}.

Electron-density maps were calculated for HRV14 using the native phases derived from monochromatic data, and structure factors corresponding to $F_{\text{Laue}} - F_{\text{Mono}}$ (difference map) and $F_{\text{Laue}} - wF_{\text{Mono}}$ (weighted map) (Johnson, 1978). No electron-density maps were calculated using CPV data. The maps were symmetry averaged according to the 20-fold non-crystallographic icosahedral symmetry of the virus particles. The binding pocket of HRV14 is not necessarily occupied in every one of the 60 protomers. The weight w allowed for subtraction of the structure-factor component corresponding to the virus still in native conformation (Badger, Minor, Oliveira, Smith & Rossmann, 1989; Chapman, Minor, Rossmann, Diana & Andries, 1991) and also corrected for bias from the used of native phases (Luzzati, 1953). The value of w was chosen so that the antiviral compound density was approximately the same height as the density representing viral protein. A difference map with $w = 1$ is a good indication of the signal strength. Such a map should show the region of conformational differences relative to the surrounding noise. A map with a suitably chosen weight $0.5 < w < 1$ should show the actual structure of the virus complex or the mutated virus and, therefore, is easier to interpret.

Results

CPV

CPV is a single-stranded DNA virus whose atomic structure has been determined to 3.0 Å resolution. The crystals are polymorphic with four characterized crystal forms and two known atomic structures (Tsao *et al.*, 1991; Wu, Keller & Rossmann, 1993). Indexing of the Laue diffraction photographs for CPV prove difficult. Two of the photographs were eventually indexed in a tetragonal space group $P4_32_12$ using cell dimensions $a = 256.6$ and $c = 805.0$ Å (Wu *et al.*, 1993). It was not possible to index the third and best diffraction image, probably because the crystal had a unit cell not previously characterized. Table 2 shows some of the data-processing statistics for the indexed photographs. The completeness of the data dropped below 2% beyond 4.2 Å resolution (Fig. 4). The data extracted from the photograph were not sufficient to calculate an electron-density map.

CPV showed particular radiation sensitivity in a polychromatic X-ray beam. Only three photographs from a total of 26 exposed showed diffraction of reasonable quality. Even short exposures (in the order of 10 s) resulted in streaked photographs, indicating high mosaicity. The long streaks seen on longer exposures are indicators of the crystal deterioration in the X-ray beam.

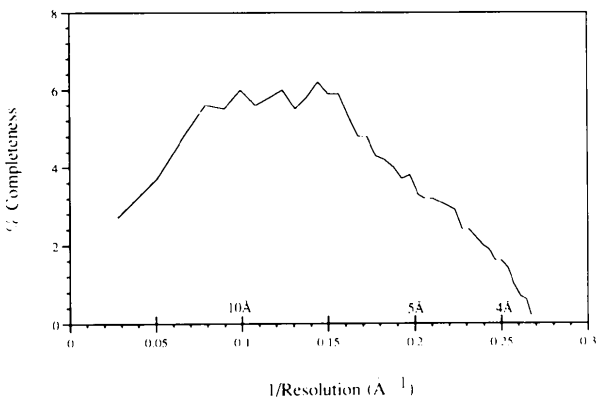

Fig. 4. Completeness of unique data as a function of resolution for canine parvovirus. The total number of reflections observed was 33 107. The number of unique reflections was 8896. Only singlets were included. Data were predicted to 3.5 Å resolution.

The difference between the quality of the diffraction photographs taken with short exposures times and high beam intensity (some interpretable diffraction) compared to longer exposure times and lower beam intensity (extreme streaking) emphasizes that the length of time elapsed from first exposure is at least as important as the X-ray dosage. To collect a useful data set multiple exposures would have had to be taken. This is not at all in line with the aspirations of collecting a data set from a minimal number of crystals. For this virus there was no advantage to continuing with the Laue diffraction trials.

*HRV*14

HRV14 is a single-stranded RNA virus whose structure has been refined to 3.0 Å resolution (Arnold & Rossmann, 1989). The capsid consists of 60 protomers each made up from four structural proteins VP1–VP4 with relative molecular masses of 32 000, 29 000, 26 000 and 7 000, respectively. The major surface proteins VP1–VP3 are rather similar in structure with differences mainly in the loops joining the β-strands (Rossmann *et al.*, 1985). The fourth protein, VP4, is much smaller than the other three and lies largely in the interior of the particle. The major feature on the surface of the virus is a deep cleft, or 'canyon', which separates the major part of the VP1 subunit from VP2 and VP3 and thus forms a channel 25 Å deep and 12–30 Å wide around the fivefold axes of the icosahedral particle (Fig. 1). All of the antiviral compounds studied so far in complex with HRV14 bind into a hydrophobic pocket within the VP1 β-barrel under the canyon, and the resulting conformational changes in each case are found to be similar (Badger *et al.*, 1988; Badger, Minor *et al.*, 1989; Chapman *et al.*, 1990; Chapman *et al.*, 1991; Kim *et al.*, 1993; Smith *et al.*, 1986).

HRV14 crystals were prepared according to Arnold *et al.* (1984). The crystals are cubic with cell dimensions $a = b = c = 445.1$ Å and belong to space group $P2_13$. Each unit cell contains four virus particles situated with an icosahedral threefold axis along the body diagonal of the unit cell, allowing for 20-fold symmetry averaging of the electron-density maps. The Laue data processing is reported in Table 3 and was more successful than that for CPV. Electron-density maps were calculated, and displayed using the program *FRODO* (Jones, 1978). Their quality was assessed by comparison with electron-density maps and atomic coordinates derived from monochromatic data for the same antiviral compounds (Table 4) (Chapman *et al.*, 1991; Kim *et al.*, 1993). In addition, a mutation Leu2170* to Val can be used to monitor map quality. The mutation occurred spontaneously in the passaging of the wild type HRV14 virus some time in early 1985 after the native data had been collected. All difference maps relative to the native data should have a negative peak in this position. The appearance of this peak therefore acts as a good indicator for the quality of the map.

The binding pocket as modeled using monochromatic data for HRV14 complexed with WIN 54954 is shown in Fig. 5. The largest structural changes on compound binding are seen in the strand βH leading into the GH loop (residues 1210–1247), which moves up to 4.5 Å

* In the four-digit identifier for each residue, the first digit designates viral proteins 1–4 while the next three are the residue sequence number.

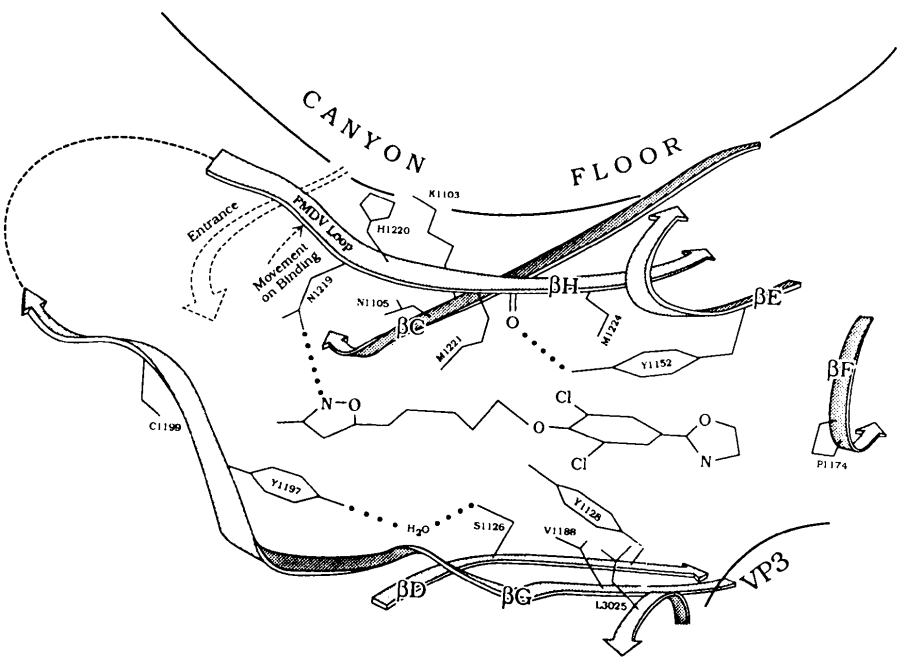

Fig. 5. A diagrammatic representation of the antiviral compound binding environment in HRV14. The compound WIN 54954 is shown in the diagram (Chapman *et al.*, 1990).

away from its position in the native structure to relieve steric conflict between Met1221 and the antiviral compound. His1220 moves to protrude further into the canyon. Asn1219 moves closer to the WIN compounds to make a putative hydrogen bond. The neighbouring strands βE from residues 1150 to 1156 and βC from residues 1100 to 1107 shift in the same direction. Tyr1152 rotates slightly and moves about 1 Å away from the antiviral compound. At the other side of the antiviral compound binding pocket Tyr1128 moves away from the antiviral compound, and in certain compounds makes a hydrogen bond. Tyr1197, at the solvent-accessible end of the pocket, also shifts. Val1188 rotates away from the antiviral compound and residues on either side of it are displaced slightly.

WIN 54954 is a member of a series of oxazolinyl isoxazoles developed by the Sterling Winthrop Research Institute. It is a WIN compound of intermediate length, with the central aliphatic chain containing five methylene groups (Fig. 6*a*). Symmetry-averaged difference electron-density maps were calculated using the native phases and structure factors corresponding to $F_{\text{Laue}} - F_{\text{Mono}}$ and $F_{\text{Laue}} - 0.85F_{\text{Mono}}$. The maps were not clear enough to allow extensive modeling. In the difference map the peaks at the site of the anticipated conformational changes were about the same height as 'noise' peaks. Nevertheless the largest continuous peak in the map was identifiable as being caused by the antiviral compound. The conformational changes that take place on binding have been modeled from monochromatic electron-density maps at 3.0 Å resolution and were used in assessing the Laue electron-density maps. Continuity of the polypeptide chain electron density was poor in the weighted map. The maps showed the antiviral compound position, conformational changes of a few of the bulky side chains and the major main-chain movements (Table 4).

R 61837 is an antirhinoviral compound developed by the Janssen Research Foundation in Belgium (Fig. 6*c*). The antiviral compound has two major differences in chemical composition from the WIN compounds. It is shorter than most WIN compounds and has a bulky piperazine ring in the central position where the WIN compounds have an aliphatic chain. This makes the compound less flexible in the pocket but gives greater opportunity for interactions to improve binding affinity. A difference map and a weighted map with $w = 0.75$ were calculated. The difference map shows the presence of the antiviral compound clearly (Table 4). The difference map and the weighted map were used in combination to remodel the virus structure in the antiviral compound binding pocket. The density indicates that the piperazine ring at the centre of the structure adopts a chair conformation rather than a 'boat' conformation. The continuity of the electron density representing the polypeptide chain in the weighted map was better than for WIN 54954. The electron-density maps permitted modeling of the large-scale changes without reference to the monochromatic structure (Chapman *et al.*, 1991; Kim *et al.*, 1993), which later confirmed the changes identified in the Laue maps (Table 4).

R 77975 was also supplied by the Janssen Research Foundation in Belgium (Fig. 6*d*). A difference map and a weighted map with $w = 0.7$ were calculated (Fig. 7). The positive density in the weighted map corresponds to the antiviral compound adopting a chair conformation for the central ring. The antiviral compound binds in the same orientations as R 61837, which can be determined by comparing the density of the ethoxy group with the pyridazine group. The continuity of the electron density representing the polypeptide chain in the weighted map was quite good, consistent with the fourfold increase in

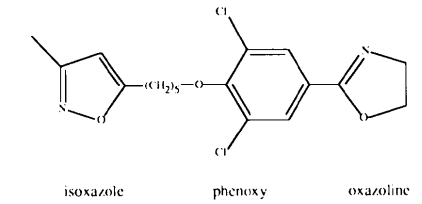

WIN 54954

(*a*)

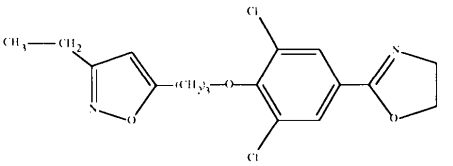

WIN 61876

(*b*)

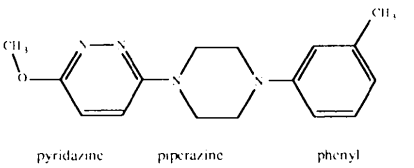

R 61837

(*c*)

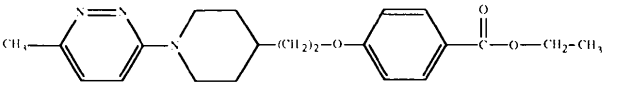

R 77975

(*d*)

Fig. 6. The antiviral compounds studied in complex with HRV14 using Laue diffraction. The compounds with the prefix WIN were provided by the Sterling Winthrop Research Institute and those with the prefix R were provided by the Janssen Research Foundation. The left end of these compounds is situated close to the pocket entrance, while the right end is deep within the pocket. Their orientation in this figure roughly corresponds to the side view from A in Fig. 1.

Table 4. *Interpretation of electron-density maps in the vicinity of the hydrophobic pocket and of the standard mutation*

	Monochromatic result	WIN 54954	R 61837	R 77975	WIN 61876
Compound orientation	Flattened rings. Substituents clear.	Interpretable because of chlorine bulges.	Slight flattening of rings. Shoulder on density shows position of phenyl methyl.	Rings flattened to show faces.	Bulk of phenoxy with chlorine substituents determines orientation.
Completeness of compound cover in weighted map	Full.	Poor, density lacking for aliphatic chain.	Slightly short.	Quite good – aliphatic chain visible. One shoulder of compound a little sparse.	Quite good – slightly short. Density a little sparse for one chlorine.
GH loop (1210–1247)	1219 shows binding.	Poor density.	Poor density.	Main chain and side chains patchy.	Quite good – main chain and most side chains have density.
His1220	Good density.	Difference map shows positive density for main chain.	Weighted map shows bulge for side chain. Main chain good.	Difference map not clear. Weighted map shows truncated side-chain density.	Good density both in difference and weighted maps.
Met1221	Good density.	Just negative density where native lies.	Difference map okay. Short side-chain density.	Weighted map shows density almost to end of side chain.	New position clear. Side chain extends towards compound.
Tyr1152	Good. Shows binding to some compounds.	Poor.	Small positive and negative peaks to show movement.	Weighted map shows strong density with connectivity to the compound.	Clear positive and negative peaks in difference density.
Tyr1128	Good. Shows binding to some compounds.	Weighted map shows binding to compound.	Small shifts indicated in difference map. Binding indicated in weighted map.	Good density. No connectivity to compound.	Clear density. No binding visible in this compound.
Tyr1197	Good.	Some density for side chain in weighted map. No sign of binding.	Weighted map shows connectivity to compound.	Good density. Shows connectivity to compound.	Clear density – no connectivity to this compound. Apparently stacking edge on with 1190.
Val1188	Small shift observed.	No density.	No density.	Small negative peak in difference map.	Small negative peak in difference map.
Water	Visible.	Not visible.	Not visible.	Not visible.	Not visible.
L2170→V	Strong difference peak.	Difference peak just above noise.	Difference peak highest peak in mutation region, but rather weak.	Difference peak clear.	Difference peak highest peak in mutation region.

the number of reflections at low resolution. The quality of the map was assessed by comparison to a well determined structure of the complex (Kim *et al.*, 1993). The large-scale conformational changes were easily identified. More small-scale changes could be interpreted with confidence, possibly because some 3.5 Å resolution data could be included in the electron-density map calculation.

WIN 61876 is similar to WIN 54954 (Fig. 6*b*). The two major differences in their structures are that the aliphatic chain has three members not five, and the methylphenyl ring is replaced by an ethylphenyl ring. Two photographs were processed for this antiviral compound and the data were combined into a single data set (Table 3). A difference map and a weighted map with $w = 0.7$ were calculated (Fig. 8). The difference map showed electron density corresponding to the antiviral compound with the largest peak height in the region of the pocket, at approximately twice the height of the largest noise peaks. The weighted electron-density map for this antiviral compound was easier to interpret than the earlier maps and the side chains are better defined. The electron density representing the main chain of the protein is largely continuous and most of the side chains are represented in the binding pocket. The electron density indicates that the conformational changes which occur upon HRV14 binding this antiviral compound are very similar to those which occur upon binding of WIN 54954. The aliphatic chain, which is two members shorter, appears to adopt a more elongated conformation, allowing the bulky groups at either end of the compound to lie in the same position as for WIN 54954. There appears to be room to accommodate the extra methyl group on the phenyl ring without additional conformational change. These results were later found to be consistent with analysis of monochromatic data (unpublished results).

In addition to the antiviral compound binding studies, diffraction photographs were taken from crystals of two different drug-resistant mutants of HRV14 (Table 1)

selected by propagating the virus in the presence of an antiviral compound (Badger, Krishnawamy *et al.*, 1989; Heinz *et al.*, 1989). None of the photographs from one of the mutants were processable. The amount and quality of data obtained from each photograph of the other mutant, Cys1199 to Phe, varied. The data from the best two films, judged by number of reflections and the wavelength normalization merging R factor, were chosen for use in the calculation of a difference map (Table 3). The difference map calculated from this Laue data shows a large negative peak in the position of residue 2170, indicating the change from leucine to valine (Fig. 9), which is the only significant peak on the map. The height of this negative peak over the r.m.s. density was 4σ, larger than it was in the various antiviral compound difference electron-density maps (Table 4). There was no sign of the mutation Cys1199 to Phe which should be found at the entrance to the antiviral compound binding pocket. The virus sequence was therefore re-analyzed, confirming that the crystals were of a native virus whose only difference to the original wild type was at position 2170. These results thus indicated the good quality of the Laue data, showing a single mutation very clearly and identifying an error in the anticipated sequence.

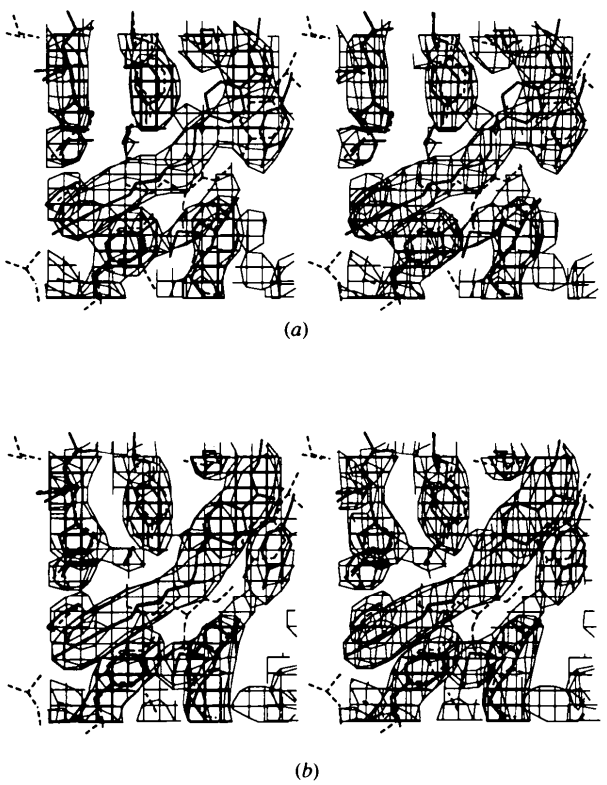

Fig. 7. Weighted electron-density map $(F_{\text{complex}} - wF_{\text{native}})\exp(i\alpha_{\text{native}})$ calculated from (*a*) Laue diffraction data ($w = 0.7$) and (*b*) monochromatic diffraction data ($w = 0.65$) showing the antiviral compound R 77975 in complex with HRV14. The electron-density contour level is approximately 1σ. The orientation of the binding pocket corresponds to its orientation in the icosahedral asymmetric unit in Fig. 1. The coordinates of the complex are shown in solid lines, and those of the native structure in dotted lines. In the map calculated from Laue diffraction data, density representing the viral protein is almost continuous and the density representing the compound is complete except for a small amount of density missing on the shoulder. The electron-density diagrams were prepared using the program *Molview* (Smith, 1993).

Discussion

The Laue method has been shown capable of determining small differences in structure between proteins (Duke, Wakatsuki, Hadfield & Johnson, 1994; Fulop *et al.*, 1994; Lindahl, Liljas, Habash, Harrop & Helliwell, 1992; Singer, Smalås, Carty, Mangel & Sweet, 1993). In the compound-binding studies presented here, the proportion of unique data obtained from a single Laue exposure was comparable to that obtained from a number of monochromatic exposures in a typical drug-binding study, albeit of somewhat lower resolution. The electron-density maps obtained from Laue diffraction data contained many features which compared with those in maps derived from monochromatic diffraction data. They could be used for interpreting major conformational changes, or for detecting the absence of a single methyl group.

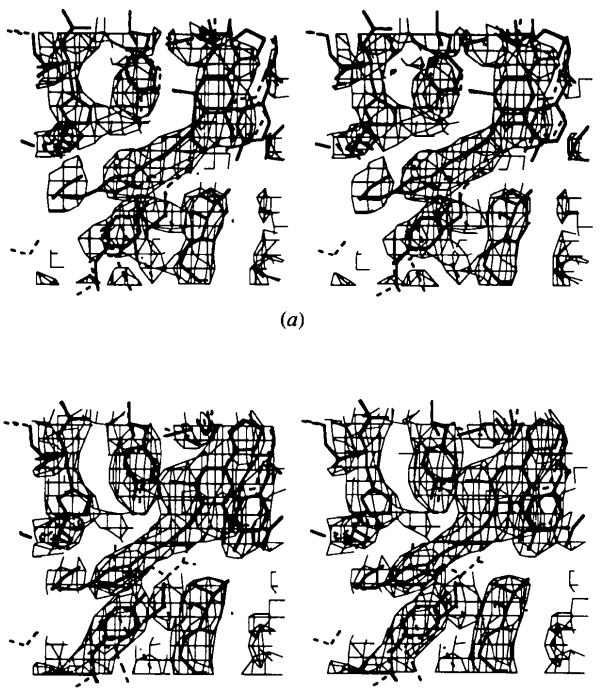

Fig. 8. The same as for Fig. 7 but for the antiviral compound WIN 61876. The electron density is missing for one of the Cl atoms substituting the phenyl ring and the density is a little short compared to the electron density in the map calculated from monochromatic data.

Table 5. *Summary of Laue studies performed on HRV*14

	WIN 54954	R 61837	R 77975	WIN 61876	Mutant
Synchrotron	SRS	SRS	SRS	SRS	CHESS
λ range (number of octaves)	0.3–2.1 (3.1)	0.3–2.1 (3.1)	0.45–1.7 (1.9)	0.45–1.7 (1.9) 0.3–1.5 (2.3)	0.7–1.4 (1.0)
Exposure (s)	10	4	3 × 1.5	3 × 1.5 3 × 2.3	3 + 4
Spots predicted	148367	128842	215880	235390 224684	60451 63993
% Unique predicted	58	61	54	54, 57	31, 32
Pack scaling performed?	Yes	Yes	No	No	No
R_L (λ scaling)*	26.7	20.3	15.5	15.5, 17.8	15.7, 13.4
D_{min} (Å)	4.0	3.8	3.5	3.5	3.5
% Completeness (∞–D_{min})	7.4	8.7	12.6	19.6	12.6
No. of reflections	10512	15603	34015	50729	36248
R_M (scaling to native)†	15.6	12.8	11.2	10.8	9.6
$\rho/\sigma(\rho)$ compound‡	1.5	2	2.5§	2.5§	—
$\rho/\sigma(\rho)$ mutation¶	2	2	3	3§	4§

* R_L (see Table 3).

† R_M (see Table 3).

‡ $\rho/\sigma(\rho)$ compound is the maximum electron-density peak height in the compound region compared to the r.m.s. value in the rest of the map in the difference map.

§ Highest difference peak in the area.

¶ $\rho/\sigma(\rho)$ mutation is the maximum electron-density peak height in the region of a mutation L2170 to V compared to the r.m.s. value in the rest of the map in the difference map.

Previous studies have demonstrated the importance of the low-resolution data which is largely inaccessible using the Laue geometry (Duke *et al.*, 1992; Lindahl *et al.*, 1992). This is particularly apparent in its effect on the continuity of electron density. In the electron-density maps presented here this was also observable. However 20-fold symmetry averaging (in the case of HRV14) compensates, to a certain extent, for the lack of low-resolution data. Thus, electron-density maps calculated with only 12% of the complete data in the resolution range 15–3.5 Å, and with significantly lower completeness between 15 and 7 Å resolution, had very reasonable continuity. The proportion of low-resolution singlet reflections can be maximized by restricting the wavelength range to an octave ($\lambda_{min} = \lambda_{max}/2$) (Cruickshank, Helliwell & Moffat, 1987), which was roughly the case for the CHESS data.

Restricting the wavelength range of the incident radiation had a marked effect on both the number of images that recorded usable data and the quality of those data (Table 5). At short wavelengths the lower intensity of the X-ray beam, the reduced scattering power of the crystal and the slower response in the film combined to make the reflections weak. Thus, in general, the high-energy part of the spectrum contributed to radiation damage while not providing much useful diffraction data (Table 6). Many of the high-resolution reflections are predicted at these short wavelengths. A major determinant in the quality and interpretability of the electron-density maps calculated from Laue diffraction data is the effective resolution limit of the data. Since the high-resolution reflections are weaker, the resolution limit is due, in part, to the inability to collect reasonably long exposures before radiation damage becomes critical. It was found that the wavelength range over which data were collected can play a significant role in determining whether high-resolution reflections were going to be measurable.

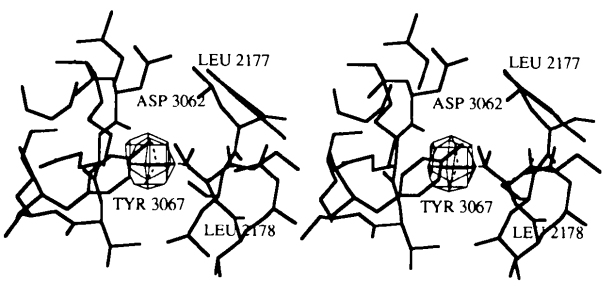

Fig. 9. Negative difference electron density in the vicinity of the mutation L2170 to V. The largest negative peak was two times bigger than any other positive or negative peak. The dashed lines represent the original leucine structure.

The success rate for taking processable photographs was greater when using a restricted wavelength range. Furthermore, the data had a higher signal-to-noise ratio than data collected using a broader bandpass (Fig. 3, Table 5) and there was an increase in the proportion of low-resolution reflections because there were fewer multiplets (Fig. 10) (Cruickshank *et al.*, 1987). It is notable that the same percentage of the total unique data set was obtained from the images with a restricted wavelength range, where the predicted proportion of the data set on a single image was rather less. This is because of both the increase in number of singlet reflections on such films and the benefits of collecting a smaller number of reflections (and, therefore, fewer spatial overlaps) within a narrower dynamic range. The number of reflections that were successfully extracted from the Laue photographs was not substantially more (approxi-

Table 6. *Number of reflections and average intensity in resolution and wavelength bins for film No.* 17 *HRV*14 + *WIN* 61876

Each entry consists of the number of measured reflections below which is shown their average intensity on a relative scale.

λ	Resolution range (Å)						
Range (Å)	20.00	10.00	6.00	4.00	3.70	3.50	Totals
0.30–0.35	19	256	1645	7411	3068	2723	15122
	111	33	37	45	43	47	44
0.35–0.40	16	242	1666	7251	3149	2931	15255
	313	68	46	54	56	59	55
0.40–0.45	19	261	1642	7154	3355	3101	15532
	326	129	62	64	68	72	68
0.45–0.50	17	273	1655	7272	3474	3159	15850
	565	167	65	73	84	89	80
0.50–0.55	19	266	1639	7468	3434	3083	15909
	579	152	66	79	98	106	89
0.55–0.60	11	236	1637	7547	3457	3271	16159
	663	249	79	95	117	99	102
0.60–0.65	0	2	829	7645	3535	3349	15360
		688	89	114	92	76	99
0.65–0.70	0	2	868	7720	3594	3384	15568
		881	106	118	81	79	100
0.70–0.75	0	0	887	7884	3672	2623	15066
			131	120	85	91	107
0.75–0.80	0	0	917	7938	2779	270	11904
			146	125	96	87	119
0.80–0.85	0	0	899	7706	442	0	9047
			168	133	98		135
0.85–0.90	0	0	910	6022	0	0	6932
			194	147			153
0.90–0.95	0	0	909	4459	0	0	5368
			174	131			138
0.95–1.00	0	0	903	3296	0	0	4199
			164	114			124
1.00–1.05	0	0	970	2412	0	0	3382
			148	117			126
1.05–1.10	0	0	932	1580	0	0	2512
			147	121			131
1.10–1.15	0	0	938	948	0	0	1886
			138	119			128
1.15–1.20	0	0	925	509	0	0	1434
			141	115			132
1.20–1.25	0	0	888	141	0	0	1029
			142	113			138
1.25–1.30	0	0	746	1	0	0	747
			136	54			136
1.30–1.35	0	0	462	0	0	0	462
			142				142
1.35–1.40	0	0	237	0	0	0	237
			132				132
1.40–1.45	0	0	76	0	0	0	76
			152				152
1.45–1.50	0	0	3	0	0	0	3
			159				159
Totals	101	1538	23183	102364	33959	27894	
Averages	408	134	108	100	83	80	0

mately twice in the better results here) than for a monochromatic image, but the Laue data are spread more uniformly over reciprocal space, except in the low-resolution hole. The two photographs of HRV14 complexed with WIN 61876 were taken with radiation that had a similar spread of wavelengths but in different ranges. The photograph (No. 30) taken using longer wavelengths was slightly better [see for example wavelength-scaling factor (R_L), Table 3]. Although longer wavelengths cause greater radiation damage, nevertheless the better response of film and the greater scattering power of the crystals at these wavelengths increases the quality of the data (Fig. 3). The wavelength range over which data were collected affected the number of crystals which gave interpretable diffraction, the resolution to which diffraction data could be measured and the signal-to-noise ratio of the data. The results presented here support the proposal of Sweet and co-workers (Sweet, Singer & Smalås, 1993) that data should be collected using a wavelength range that is limited to only one octave (Table 5, Fig. 3 and 10).

The ratio of the number of crystals used to the number of processable films obtained was rather low (Table 1). In particular, the sensitivity of CPV crystals to the intensity of beam rendered most of the diffraction images uninterpretable, indicating that this method of data collection is not well suited to crystals which have a tendency towards disorder. One problem is that the same mosaic spread causes a larger spot size on the detector for polychromatic than for monochromatic radiation (Fig. 11). The high-energy incident on a crystal used for Laue diffraction causes rapid radiation damage and, therefore, increased mosaic spread. In addition, increase in mosaicity increases the overlap of individual reflections. Use of staggered exposures presumably reduced crystal overheating and, therefore, mosaic spread. Crystals of plant and insect viruses seem to be more resistant than animal viruses to environmental effects. For instance, up to about five Laue photographs could be taken from TBSV (Campbell *et al.*, 1990) or Flock house virus (Clifton, 1992) before serious radiation damage set in. There may be a link between these properties and the fact that these viruses have to withstand substantially larger variations in pH, temperature, ionic strength and humidity during their life cycle compared to many animal viruses. Flash freezing of crystals could be very beneficial in the collection of Laue data, permitting

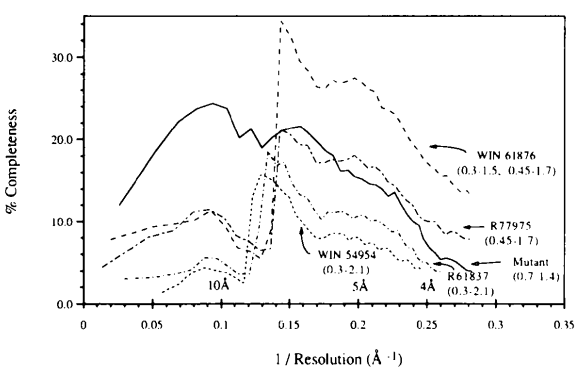

Fig. 10. Completeness of unique data as a function of resolution for the virus Laue data sets processed, using singlet data only. The mutant data were most complete at low resolution and were collected with the most restricted wavelength range. WIN 61876 and R 77975 were collected using a shorter wavelength range than the other two antiviral compounds. The resolution of the data improved and the proportion of low-resolution data extracted increased as a result of limiting the wavelength range of data collection, and changing the method of exposure.

exposure to a high-intensity beam without serious radiation damage. However, since a small mosaic spread is of critical importance, conditions for freezing would have to be found that did not cause a mosaic increase. It is an unfortunate side effect in many cryocrystallographic experiments that the mosaicity of the crystal increases upon freezing.

The detector chosen for a Laue diffraction experiment is also critical. The recorded intensity of short-wavelength data could be improved using image plates, which are more sensitive in this wavelength range (Sakabe, 1987). The current drawback in the use of image plates is lack of spatial resolution. In the case of virus data collection, 200 000 reflections can be predicted over the area of a film. Even using the minimum wavelength spread of one octave, over 60 000 reflections were predicted. An image plate with 2000 × 2000 pixels would not have sufficient pixels to resolve or deconvolute this number of reflections, even if the plate was moved further back to decrease the degree of overlap. As the spatial resolution of both image plates and CCD detectors improves, these could have a significant role in the successful collection of Laue diffraction data from crystals with large unit cells.

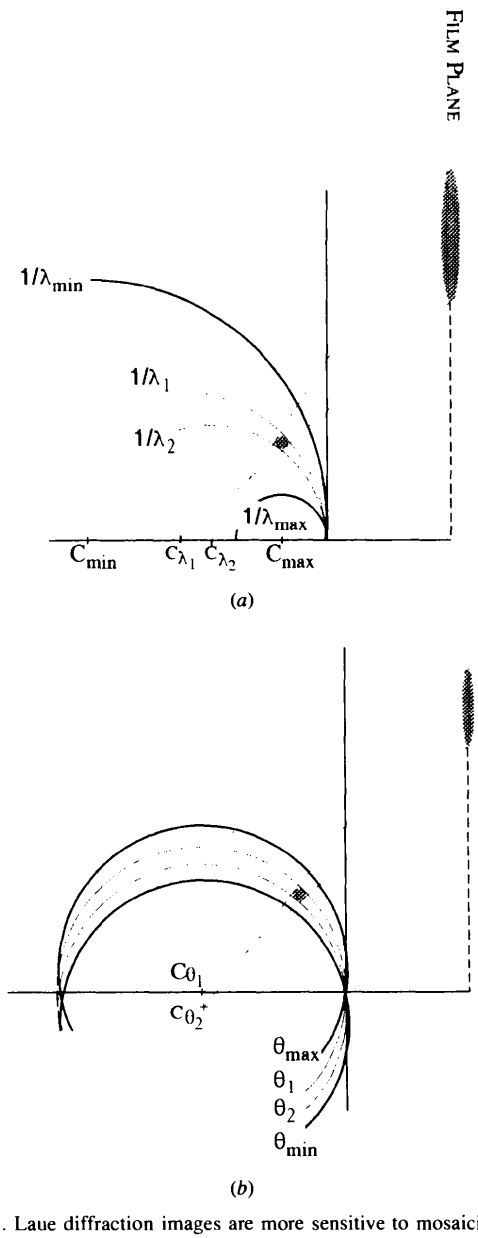

Fig. 11. Laue diffraction images are more sensitive to mosaicity. The mosaicity of a crystal is represented here by a reciprocal lattice point of finite size. (*a*) In the case of Laue diffraction a reflection diffracts over a wavelength range (λ_1 to λ_2). C_{min}, C_{λ_1},C_{λ_2} and C_{max} are the centres of Ewald spheres with radii $1/\lambda_{max}$, $1/\lambda_1$, $1/\lambda_2$ and $1/\lambda_{min}$, respectively. The diffraction limits at λ_{max} and λ_{min} are shown in bold lines. (*b*) In the monochromatic case diffraction will occur as the crystal lattice passes through a shell with radius $1/\lambda_1$ from Bragg angle θ_1 to θ_2. The oscillation of the crystal is represented by the rotation of the shell around the origin. C_{θ_1} and C_{θ_2} are the centres of an Ewald sphere with radius $1/\lambda_{max}$ at angles of θ_1 and θ_2, respectively. The limits of the oscillation at θ_{max} and θ_{min} are shown in bold lines.

The authors would like to thank Koen Andries, Janssen Research Foundation, and Mark McKinlay, Sterling Research Inc., for providing the antiviral compounds; Trevor Greenhough and Annette Shrive for assistance with data collection; Marcia Kremer for crystals of HRV14; and Mavis Abandje for crystals of CPV. AH and JH were supported by the Medical Research Council, England. The work was also supported by grants from Sterling Research Inc. and the National Institute of Health to MGR as well as the Markey Foundation for the development of structural studies at Purdue University.

References

ARNOLD, E., ERICKSON, J. W., FOUT, G. S., FRANKENBERGER, E. A., HECHT, H. J., LUO, M., ROSSMANN, M. G. & RUECKERT, R. R. (1984). *J. Mol. Biol.* **177**, 417–430.

ARNOLD, A. & ROSSMANN, M. G. (1989). *J. Mol. Biol.* **211**, 763–801.

ARNOLD, E., VRIEND, G., LUO, M., GRIFFITH, J. P., KAMER, G., ERICKSON, J. W., JOHNSON, J. E. & ROSSMANN, M. G. (1987). *Acta Cryst.* A**43**, 346–361.

BADGER, J., KREMER, M. J., OLIVEIRA, M. A., SMITH, T. J., GRIFFITH, J. P., GUERIN, D. M. A., KRISHNAWAMY, S., LUO, M, ROSSMANN, M. G., MCKINLAY, M. A., DIANA, G. D., DUTKO, F. J., FANCHER, M., RUECKERT, R. R. & HEINZ, B. A. (1988). *Proc. Natl Acad. Sci. USA*, **85**, 3304–3308.

BADGER, J., KRISHNAWAMY, S., KREMER, M. J., OLIVEIRA, M. A., ROSSMANN, M. G., HEINZ, B. A., RUECKERT, R. R., DUTKO, F. J. & MCKINLAY, M. A. (1989). *J. Mol. Biol.* **207**, 163–174.

BADGER, J., MINOR, I., OLIVEIRA, M. A., SMITH, T. J. & ROSSMANN, M. G. (1989). *Proteins*, **6**, 1–19.

CAMPBELL, J. W., CLIFTON, I. J., GREENHOUGH, T. J., HAJDU, J., HARRISON, S. C., LIDDINGTON, R. C. & SHRIVE, A. K. (1990). *J. Mol. Biol.* **214**, 627–632.

CHAPMAN, M. S., GIRANDA, V. L. & ROSSMANN, M. G. (1990). *Semin. Virol.* **1**, 413–427.

CHAPMAN, M. S., MINOR, I., ROSSMANN, M. G., DIANA, G. D. & ANDRIES, K. (1991). *J. Mol. Biol.* **217**, 455–463.

CLIFTON, I. J. (1992). D. Phil thesis, Univ. of Oxford, England.

CLIFTON, I. J., CRUICKSHANK, D. W. J., DIAKEN, G., ELDER, M., HABASH, J., HELLIWELL, J. R., LIDDINGTON, R. C., MACHIN, P. A. & PAPIZ, M. Z. (1985). *J. Appl. Cryst.* **18**, 296–300.

CLIFTON, I. J., ELDER, M. & HAJDU, J. (1991). *J. Appl. Cryst.* **24**, 267–277.

CRUICKSHANK, D. W. J., HELLIWELL, J. R. & MOFFAT, K. (1987): *Acta Cryst.* A**43**, 656–674.

DUKE, E. M. H., HADFIELD, A. T., WALTERS, S., WAKATSUKI, S., BRYAN, R. K. & JOHNSON, L. N. (1992). *Philos. Trans. R. Soc. London Ser. A*, **340**, 245–261.

DUKE, E. M. H., WAKATSUKI, S., HADFIELD, A. T. & JOHNSON, L. N. (1994). *Protein Sci.* **3**, 839–842.

FULOP, V., PHIZACKERLEY, P., SOLTIS, M., CLIFTON, I. C., WAKATSUKI, S., ERNME, J., EDWARDS, S. L. & HAJDU, J. (1994). *Structure*, **2**, 201–208.

GREENHOUGH, T. J. & SUDDATH, F. L. (1986). *J. Appl. Cryst.* **19**, 400–409.

HADFIELD, A. T. (1992). D. Phil thesis, Univ. of Oxford, England.

HAJDU, J., GREENHOUGH, T. J., CLIFTON, I. J., CAMPBELL, J. W., SHRIVE, A. K., HARRISON, S. C. & LIDDINGTON, R. C. (1989). *Synchrotron Radiation in Structural Biology*, edited by R. M. SWEET, pp. 331–339. New York: Plenum Press.

HEINZ, B. A., RUECKERT, R. R., SHEPARD, D. A., DUTKO, F. J., MCKINLAY, M. A., FANCHER, M., BADGER, J. & ROSSMANN, M. G. (1989). *J. Virol.* **63**, 2476–2485.

HELLIWELL, J. R., HABASH, J., CRUICKSHANK, D. W. J., HARDING, M. M., GREENHOUGH, T. J., CAMPBELL, J. W., CLIFTON, I. J., ELDER, M., MACHIN, P. A., PAPIZ, M. Z. & ZUREK, S. (1989). *J. Appl. Cryst.* **22**, 483–497.

JOHNSON, J. E. (1978). *Acta Cryst.* B**34**, 576–577.

JONES, A. T. (1978). *J. Appl. Cryst.* **11**, 268–272.

KIM, K. H., WILLINGMANN, P., GONG, Z. K., KREMER, M. J., CHAPMAN, M. S., MINOR, I., OLIVEIRA, M. A., ROSSMANN, M. G., ANDRIES, K., DIANA, G., DUTKO, F. J., MCKINLAY, M. A. & PEVEAR, D. C. (1993). *J. Mol. Biol.* **230**, 206–226.

LINDAHL, M., LILJAS, A. HABASH, J, HARROP, S. & HELLIWELL, J. R. (1992). *Acta Cryst.* B**48**, 281–285.

LUZZATI (1953). *Acta Cryst.* **6**, 142–152.

OLIVEIRA, M. A., ZHAO, R., LEE, W.-M., KREMER, M. J., MINOR, I., RUECKERT, R. R., DIANA, G. D., PEVEAR, D. C., DUTKO, F. J., MCKINLAY, M. A. & ROSSMANN, M. G. (1993). *Structure*, **1**, 51–68.

ROSSMANN, M. G., ARNOLD, E., ERICKSON, J. W., FRANKENBERGER, G., GRIFFITH, J. P., HECHT, H. J., JOHNSON, J. E., KAMER, G., LUO, M., MOSSER, A. G., RUECKERT, R. R., SHERRY, B. & VRIEND, G. (1985). *Nature (London)*, **317**, 145–153.

ROSSMANN, M. G., LESLIE, A. G. W., ABDEL-MEGUID, S. S. & TSUKIHARA, T. (1979). *J. Appl. Cryst.* **12**, 570–581.

SHRIVE A. K., CLIFTON, I. J., HAJDU, J. & GREENHOUGH, T. J. (1990). *J. Appl. Cryst.* **23**, 169–174.

SINGER, P. T., SMALÅS, A., CARTY, R. P., MANGEL, W. F. & SWEET, R. M. (1993). *Science*, **259**, 669–673.

SMITH, T. J. (1993). *J. Appl. Cryst.* **26**, 496–498.

SMITH, T. J., KREMER, M. J., LUO, M., VRIEND, G., ARNOLD, E., KAMER, G., ROSSMANN, M. G., MCKINLAY, M. A., DIANA, G. D. & OTTO, M. J. (1986). *Science*, **233**, 1286–1293.

SWEET, R. M., SINGER, P. T. & SMALÅS, A. (1993). *Acta Cryst.* D**49**, 305–307.

TSAO, J., CHAPMAN, M. S., ABANDJE, M., KELLER, W., SMITH, K., WU, H., LUO, M., SMITH, T. J., ROSSMANN, M. G., COMPANS, R. W. & PARRISH, C. R. (1991). *Science*, **251**, 1456–1464.

WAKATSUKI, S. (1993). *Data Collection and Processing*, Vol. DL/SCI/R34, edited by L. SAWYER & S. BAILEY, pp. 71–79. Warrington: SERC Daresbury Laboratory.

WU, H., KELLER, W. & ROSSMANN, M. G. (1993). *Acta Cryst.* D**49**, 572–579.